LAWRENCE
LIVERMORE
NATIONAL
LABORATORY

LLNL-JRNL-820989

Nucleon-Induced Inelastic Scattering with Statistical StrengthFunctions and the ECIS Direct Reaction Code

E. V. Chimanski, B. V. Carlson

March 30, 2021

The European Physical Journal A

Disclaimer

Eur. Phys. J. A manuscript No.
(will be inserted by the editor)

Nucleon-induced inelastic scattering with statistical strength functions and the ECIS direct reaction code

E. V. Chimanski[a,1], **B. V. Carlson**[2]

[1]Lawrence Livermore National Laboratory, Livermore, CA 94550, USA.
[2]Depto. de Física, Instituto Tecnológico de Aeronáutica - São José dos Campos, SP 12228-900, Brazil

Received: date / Accepted: date

Abstract Modern theoretical descriptions of inelastic scattering often require large numerical computational resources due to the complexity of the calculations involved. One of the most precise multi-step direct reaction approaches makes use of transition potentials obtained with sophisticated nuclear structure models. These potentials are then used in DWBA or Coupled-Channel Reaction (CCR) codes to provide numerical values for the cross section. Here we demonstrate how the complexity of such calculations might be reduced to permit easy calculation using the ECIS code, thus providing an alternative to a full computation when this becomes unfeasible even for large computers. We have studied the transition form factors within the Random Phase Approximation, where these are obtained as linear combinations of particle-hole states. At moderate to high excitation energies, where interference effects tend to disappear, we have proposed an independent particle-hole formalism in which particle-hole states are spread in energy with an appropriate strength function obtained from the RPA. The effects of more complex modes such as 2p-2h are simulated with widths calculated in a semi-classical context. Here, we verify the validity of our approximations for high-energy proton-induced reactions on ^{90}Zr target. Our calculations provide a good description of the reaction data and point toward a simplification of the description of nucleon-induced reactions based on averages of microscopic details of the projectile-target interaction.

Keywords Particle-Hole · Cross sections · Inelastic

[a]e-mail: chimanski1@llnl.gov

1 Introduction

Nuclear cross sections are key ingredients for a variety of applications from nucleosynthesis, radioisotope production for medical treatments and nuclear power plant strategies [1–3]. Theoretical reactions models are required to supplement experimental data values and sometimes to even provide them in cases where, for example, the target is a short-lived or rare isotope or when no experimental facility can perform measurements in the desired energy range.

Although inelastic multi-step direct reaction scattering models have been developed for many years, a complete description that can be directly implemented numerically is difficult to achieve. For nucleon induced reactions, simpler models introduce limited information about the nuclear structure of the target while more sophisticated approaches, when available, quickly reach a high level of complexity.

A successful approach relies on the combination of detailed nuclear structure information that can be introduced into a detailed reaction description, such as the DWBA or coupled channel theory. The RPA has been successfully employed in calculations of nucleon-induced reactions ([4,5], and for surrogate studies [6, 7]). The price of such an approach is the need for large computers to execute each step of a reaction calculation in combinations with detailed nuclear structure calculations.

In this work, we show how RPA form factors can be simplified at medium to high excitation energy by substituting statistical averages for a detailed microscopic description of the transition densities. Cross sections can be obtained for independent particle-hole configurations and then spread in energy according to the statistical distributions obtained from an analysis of the

microscopic description.
This work is organized as follows: We present a short introduction to the theoretical formalism. Next, the transition densities and the averaging scheme are presented. The numerical cross sections obtained and the concluding remarks are given in the results and conclusion sections, respectively.

2 Theoretical Formalism

For the sake of compactness, we only provide a description of the most necessary components of the calculations, while references are given for completeness. We write the radial coupled channel equation as

$$\left\{\frac{d^2}{dr^2} - \frac{l_i(l_i+1)}{r^2} - \frac{2\mu_i}{\hbar^2}U_{ii}(r) + k_i^2\right\}\psi_i(r) = \sum_{f\neq i}\frac{2\mu}{\hbar^2}U_{if}(r)\psi_f(r)\,, \tag{1}$$

where U_{if} represents the effective potential for a transition between the states i and f.
The transition potential U_{if} is induced by the interaction between the projectile and the nucleons in the target nucleus. For inelastic scattering, one usually writes the transitions from an initial ground $|0\rangle$ to a final excited state $|f\rangle$ as

$$U_{f\leftarrow 0}(\vec{r}) = \sum_n \langle f|V_{eff}(\vec{r}-\vec{r}_n)|0\rangle \tag{2}$$

where $\vec{r}_n$ represents the position of the nucleons in the target. We can connect a nuclear structure model to this formalism by simply casting the equation above into a folding-like structure

$$U_{f\leftarrow 0}(\vec{r}) = \int d\vec{r}_t V_{eff}(\vec{r}-\vec{r}_t)\rho_{f0}(\vec{r}_t), \tag{3}$$

where

$$\rho_{f0}(\vec{r}_t) = \langle f|\sum_n \delta(\vec{r}_t-\vec{r}_n)|0\rangle, \tag{4}$$

is the one-body transition density [8].
The transition potentials (3) can be used as inputs in the ECIS reaction code [9,10] for coupled channels and DWBA reaction cross section calculations.
In large-scale fully microscopic calculations, the effective interaction V_{eff} is usually taken to be a central interaction [5]. Here, we simplify this picture by assuming a contact-like interaction $V_{eff}(\vec{r}-\vec{r}_t) = v_0\delta(\vec{r}-\vec{r}_t)$, which allow us to obtain the transition potentials (3) directly from the transition density,

$$U_{f0}(\vec{r}) = v_0\rho_{f0}(\vec{r}). \tag{5}$$

In the next section we present our proposal for simplifying the transition densities, or transition form factors, based on the RPA framework. Our goal is to reduce the complexity of the non-collective RPA modes and represent them as a statistical response function of independent p-h amplitudes spread over an energy range dictated by the RPA calculation.

3 Particle-hole form factors

For this work, we have used the RPA code by Colò et al [11] to obtain the energy spectra as well as the quantities necessary to construct the transition potentials. In what follows, we provide a brief description of the RPA and the particle-hole amplitudes.
The RPA excited states are obtained from the action of the phonon creation operator

$$\hat{\theta}_x^\dagger = \sum_{mi} X_{mi}^x\hat{A}_{mi}^\dagger - Y_{mi}^x\tilde{A}_{mi}, \tag{6}$$

in the RPA ground state

$$|\mathrm{RPA}_x\rangle = \hat{\theta}_x^\dagger|\tilde{0}\rangle, \tag{7}$$

where $\hat{A}^\dagger$ ($\tilde{A}$) represents a particle-hole (time-reversed) creation operator. The indices $m,n\,(i,j)$ stand for the HF (Hartree-Fock) single-particle orbitals, which can be particle or holes with energies above or below the Fermi level, respectively. The RPA amplitudes and excitation energies are obtained by diagonalization of the eigenvalue problem

$$\begin{pmatrix} A & B \\ -B & -A \end{pmatrix}\begin{pmatrix} X \\ Y \end{pmatrix} = E_x\begin{pmatrix} X \\ Y \end{pmatrix}, \tag{8}$$

for a given value of the total angular momentum and parity J^π. The RPA matrix elements read

$$A_{mi,nj} = (E_m - E_i)\delta_{mn}\delta_{ij} + \langle mj|V|in\rangle$$
$$B_{mi,nj} = \langle mn|V|ij\rangle\,,$$

and are obtained self-consistently with same Skyrme interaction (Sly5 [12,13]) used in the mean field calculations.
The radial transition density from the ground state to an RPA excited state can be directly obtained from the RPA code and is given by

$$\rho_J^x(r) = \frac{1}{\sqrt{2J+1}}\sum_{mi} C_{mi}^x\langle m||Y_J||i\rangle\frac{u_m(r)u_i(r)}{r^2}. \tag{9}$$

where $C_{mi}^x = (X_{mi}^x + Y_{mi}^x)$ represent the contribution of the particle-hole basis to the RPA states.
For the energy modes above the low-energy collective states, we have found that the coefficients C_{mi}^x behave

statistically [14] and can be well represented by a Breit-Wigner distribution centered around the non-interacting p-h energy E_{mi}. In this energy region, one expects the transition density to vanish when averaged over a sufficiently large range of excitation energy $2\Delta E_x$ (for each value of the angular momentum),

$$\rho_x(r) \equiv \frac{1}{N}\int_{E_x-\Delta E_x}^{E_x+\Delta E_x} dE_x \rho_J^x(r) \approx 0, \tag{10}$$

where N is the number of states within the defined energy bin around E_x. This occurs as a consequence of the randomness of the phases present in the eigenvector coefficients C_{mi}^x. To verify this property, in Figure 1 we show the averaged transition density for different excitation energies. We performed an arithmetic average in a bin of $\Delta E_x = 1.5$ MeV of each excited state. One can note that the randomness assumption is not valid in the lower energy region of the spectra for states, such as the lowest 2^+ state, that are known to be collective. As the excitation energy increases, the averaged transition density tends to vanish. When the randomness

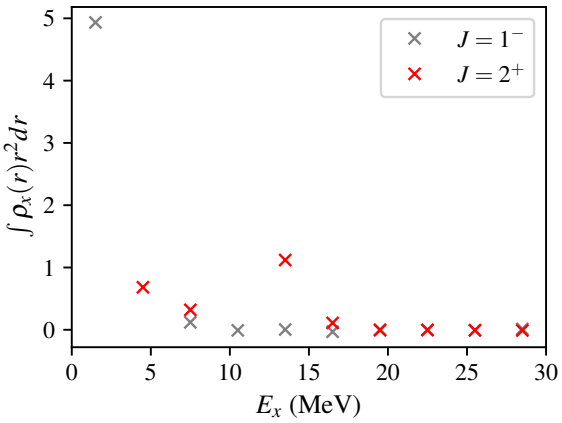

Fig. 1 Averaged RPA transition density along the excitation energy spectrum of ^{90}Zr for two values of the angular momentum and parity.

hypothesis (10) is satisfied, the p-h contributions can be represented by a Breit-Wigner distribution [14],

$$\frac{|C_{mi}^x|^2}{\Delta E_x} \equiv f_{BW}(E_x, E_{ni}) = \frac{1}{\pi\Gamma}\left[\frac{\Gamma^2}{(E_x - E_{ni})^2 + \Gamma^2}\right] \tag{11}$$

where the spreading width Γ accounts for the mixing of different p-h configurations. We will extend this later in order to account for the effects of damping into 2p-2h modes.

We show in Figure 2 a representation of the level structure of the RPA states. The vertical dark lines mark the position of the RPA energies along the horizontal energy axis. The low energy states are usually well spaced and located at energy values near or below the lower bound of the p-h basis (not shown). For the higher energy modes, the positions of the states, on average, tend to coincide with those of the unperturbed p-h basis states. In the same figure, we also show the BW strength distribution of 1p-1h nature into selected states along the spectrum. The strength of the higher energy modes is well represented by a BW distribution (Eq.11). The effects of collectivity over the enire RPA spectrum can be partially taken in to account by using an energy dependent spreading width $\gamma_{1p-1h}(E)$ [14].

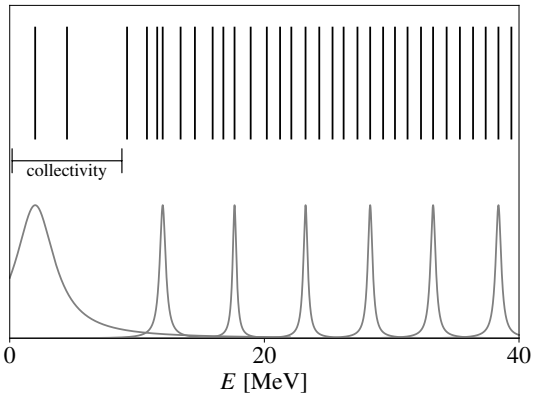

Fig. 2 Top: Schematic energy level structure of RPA states. At higher energies, the RPA states are well approximated by simple p-h modes centered around the non-interacting energy modes. Bottom: The strength contribution of the higher energy modes of the energy spectrum can be well represented by Breit-Wigner distributions (details in the text).

Taking advantage of the statistical properties of the RPA states, we use form factors (transition densities) for simple p-h configurations in the reaction formalism to obtain individual cross sections, σ_{ph}. using the ECIS code. These are then distributed along the energy spectrum according to an extended Breit-Wigner ditribution,

$$\sigma(E) = \sum_{ph}\int_{E-\Delta}^{E+\Delta} f_{BW}(E, E_{ph})\sigma_{ph} dE, \tag{12}$$

with

$$\Gamma(E) = \gamma_{1p-1h}(E) + \gamma_{2p-2h}(E) + \gamma^{\uparrow}(E) \tag{13}$$

where the first of the two widths spreads the individual cross section over the 1p-1h components. This is parametrized as $\gamma_{1p-1h}(E) = a\sqrt{E} + b\,E\,e^{\frac{-(E-E_0)^2}{2\sigma^2}}$ with $a = 4.2\times10^{-2}$ MeV^2, $b = 10^{-1}$, $E_0 = 6$ MeV and $\sigma = 5$ MeV for ^{90}Zr [14]. The 2p-2h spread width, γ_{2p-2h}, is

obtained using a semi-classical exciton-like picture, by taking into account the average squared matrix element and the density of available states (see Appendix). The escape width $\gamma^{\uparrow}$ takes into account the decay of the 1p-1h states by particle emission. The summed spreading plus escape width is used to distribute the cross sections calculated with ECIS among the bins of excitation energy spectrum $E \pm \Delta$. When using RPA form factors only the 2p-2h spreading width and the escape widths need to be employed. One notes that in the context of our model the p-h mixing can be turned off since in the limit $\gamma \to 0$

$$\lim_{\gamma \to 0} \int f_{BW}(E, E_{ph}) dE = \delta(E - E_{ph}). \tag{14}$$

Without loss of generality, we use ^{90}Zr to exemplify our approach and to compare the calculated cross sections with experimental data. In the next section, we will present the results for cross section calculations performed with the ECIS code [10,9] for proton-induced inelastic scattering at 80 MeV of incident energy.

4 Cross Section Results

We parameterize the optical potential representing the nuclear interaction between the incoming proton and the target nucleus in terms of Wood-Saxon functions

$$U_N(r) = -\frac{(V_0 + iW_0)}{1 + \exp\left[(r - R)/a_0\right]}, \tag{15}$$

where $R = r_0 A^{1/3}$ is the target radius. The necessary parameter values are obtained from the volume terms of the Koning-Delaroche optical potential [15]. The values obtained are $V_0 = 32.13$ MeV and $W_0 = 8.36$ MeV for the strengths of the real and imaginary parts, respectively, while for the geometrical parameters $r_0 = 1.21$ fm and $a_0 = 0.66$ fm^{-1} are used. The Coulomb term is taken as a uniformly charged sphere with reduced radius $r_c = 1.25$ fm. Our goal is to obtain a relatively good description of forward scattering events, since backward components tend to be small and involve two-step amplitudes, mechanisms that go beyond the formalism developed in this work, but which should be addressed in future studies.

Figure 3 presents the angular distribution for proton elastic scattering on ^{90}Zr at 80 MeV normalized to the Rutherford cross section. Although were are not able to reproduce all of the oscillatory details of the distribution, the overall is in good agreement with the experimental data. Improvements could be obtained by a fully implementation of the Koning-Delaroch optical potential.

Turning to the inelastic cross sections, we present in Fig.4 the angular distributions obtained for the individual p-h cross sections (12) using transition potentials with $v_0 = 255$ MeV as well a sthe spreading widths described above. For comparison we also show calculation performed with the RPA form factors. Both calculations provide results that follow the trend of the experimental data very well. One can see that both p-h and the RPA approaches provide similar angular distributions. As we increase the excitation energy (decrease outgoing energy), the cross section at backward angles is increasingly underestimated by our calculations. This is almost certainly due to the lack of multi-step excitation modes, which become more and more important as the excitation enegy increases but are not taken into account here. In Figure 5, we show the differential cross

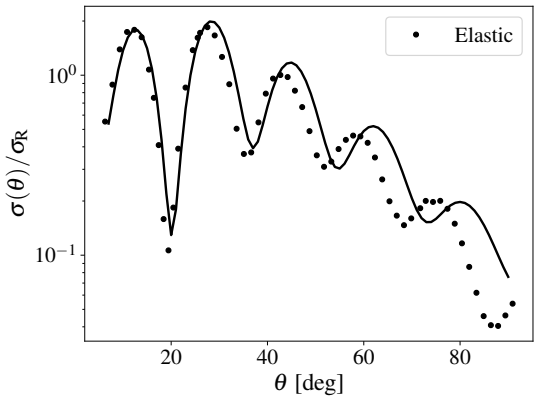

Fig. 3 Proton elastic scattering cross sections on ^{90}Zr (normalized to Rutherford cross section) at 80 MeV incident energy. The points represent experimental data taken from [16].

section at a fixed angle $\theta = 35°$ as a function of the outgoing proton energy. The reaction calculations were performed in a DWBA reaction model and take into account over 2000 form factors with angular momentum up to $J = 10$ with natural parity. The solid lines are the result of the statistical particle-hole model spread over the energy spectra using the procedure explain the previous section. The dashed lines were obtained with RPA form factors within the same DWBA basis. At lower excitation energies only the full RPA form factors can reproduce the reaction cross section strength. This is the region where interference effects play a role and the randomness assumption breaks down. For higher excitation energies, the density of p-h states increases and our model provide an excellent description of the experimental data and furnishes results very similar to those of the RPA. The large density of p-h states compensates the weak overlap of the individual states in the form factors. Before closing, we want to mention

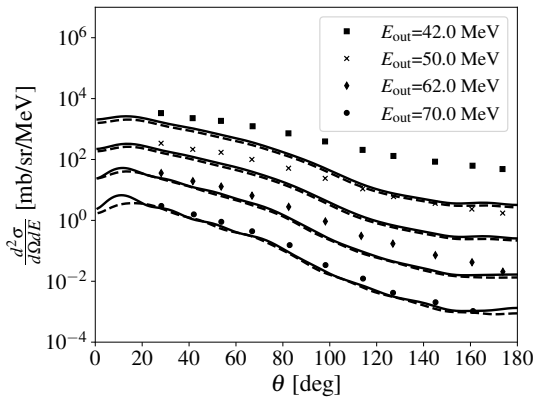

Fig. 4 Double differential angular distributions of protons incident on ^{90}Zr at 80 MeV incident for four different outgoing proton energies. Dashed and solid lines represent calculations with the RPA and independent p-h transition densities, respectively. The points represent experimental data taken from [17]. Both the data and the theoretical results are shifted starting from the bottom.

that although we could perform calculations at even higher excitation energies, one has to be careful with the different mechanisms and channels that are present in those energies. The number and complexity of the modes excited in the process increase with energy and should be carefully taken into account.

5 Concluding Remarks

In this paper we developed a reaction model based on the statistical properties of higher energy RPA modes. When randomness assumption is valid, particle-hole excitation coefficients can be well represented by a Breit-Wigner distribution centered at the non-interacting components. We employed p-h form factors to obtain cross sections in DWBA reaction calculations using the ECIS code [9,10].

Our model can be compared to the work by Dupuis [4] where a fully microscopic RPA with a Gogny interaction is employed. There, a phenomenological Gaussian distribution is used to spread the cross sections obtained from the RPA states as an attempt to estimate the damping to more complex configurations. Here, we initially spread the contribution of particle-hole modes with a distribution inspired purely by the RPA results [14]. The effects of decay to incoherent 2p-2h modes and emission are obtained in a semi-classical picture and taken into account in the spreading width.

In the future, further improvements to our calculations should be taken into account, as for example a more complete description of the optical potential. Also, a combination of different distributions could be used to better represent the lower collective energy states [18]. This could provide an effective means of accounting for the large strength of collective excitation cross sections at low excitation energies.

We would like to briefly comment on the Breit-Wigner response function we obtain for the higher energy RPA modes. In an extremely interesting numerical study of the nuclear shell model, Frazier, Brown and Zelevinsky[19] have shown that the spreading of a typical nuclear state has a Breit-Wigner form in the case of weak coupling, which transforms with the coupling strength to a Gaussian form in the physical case of strong coupling. Our response function display a Breit-Wigner form because it does not refer to typical (equilibrated) nuclear states but to 1p-1h configurations excited in a direct reaction. By comparing reaction times and equilibration times, Nishioka, Weidenmüller and Yoshida[20] argued that the initial stages of a multi-step direct reaction occur on a time scale so much smaller than the typical equilibration time of a nuclear state that a sudden approximation to the excitation could be justified. A semiclassical numerical study by Pompeia and Carlson[21] corroborated their arguments. Thus the Breit-Wigner form of the response function is due to the relative weakness of the interaction when restricted to the 1p-1h states excited in the reaction. The spreading of these states due to incoherent excitation of 2p-2h modes or particle emission is part of the equilibration process that occurs on a longer time scale, after the direct reaction has taken place.

Our principal objective here was to verify our approach before extending it to two-step amplitudes. Such an extension would address, among other features, the particles inelastically scattered to more backward angles in multi-step collisions. Modes involving 2p-2h configurations could be obtained through a two-step RPA-like process, consistent with the sudden approximation described in the preceding paragraph. Such excitation modes could be simplified to well defined distributions and their cross sections obtained directly from the ECIS code. We believe this work is thus an important step towards such a simpler approach to multi-step direct excitation processes.

Before closing, we wish to pay our respects to Dr. Jacques Raynal, author of the code ECIS, and to whom we dedicate this work. Without his lifetime of dedication to the study of direct reaction processes and the development of ECIS, studies such as this one would not be possible.

Appendix

The effects of transitions to incoherent 2p-2h modes can be estimated by the product of an averaged value of the

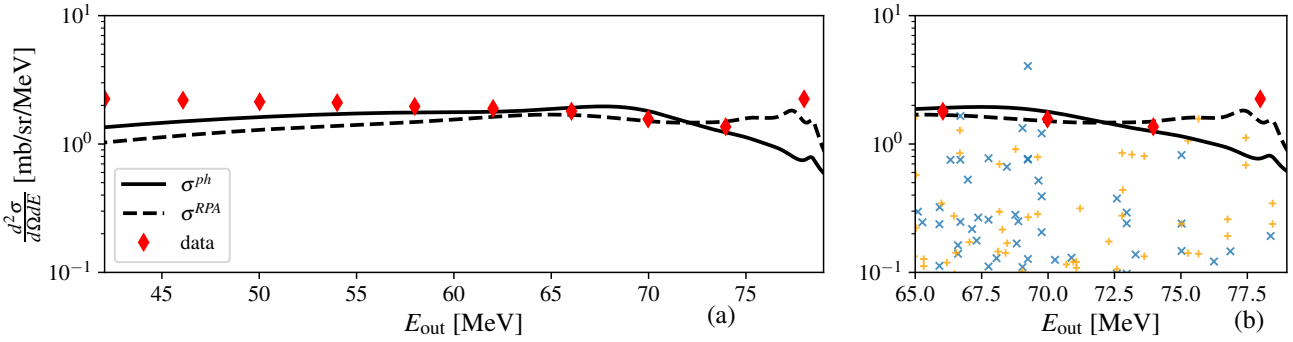

Fig. 5 (a) Double differential proton emission spectrum at $\theta = 35°$ for protons incient on ^{90}Zr at 80. Dashed and solid lines represent calculations with the RPA and the independent p-h transition densities, respectively. Red diamonds represent the experimental data taken from [17]. (b) The statistical assumption of the p-h model find its limit in the collective low energy part of the spectrum. The cross sections for each p-h and RPA state are shown as blue and orange points, respectively (color online).

squared transition matrix element times the density of available 2p-2h states $\omega(E)$,[22]

$$\gamma_{2p2h}(E) = 2\pi M^2 \omega(E), \tag{16}$$

where we use a semi-empirical parameterization of the residual interaction proposed by Koning and Duijvestijn [23] for the average squared transition matrix element,

$$M^2 = \frac{1}{A^3}\left[6.8 + \frac{4.2\times 10^5}{(E/2+10.7)^3}\right] \tag{17}$$

with E being the excitation energy and A the target mass. The density of available 2p-2h states is obtained, following Cline and Blann (with $p = 2$ and $h = 2$)[22, 24], as

$$\omega(E) = \begin{cases} \frac{(gE-1)^2}{6E} & gE > 1 \\ 0 & gE < 1, \end{cases} \tag{18}$$

where $g = A/15$ is the average single-particle level density [23]. We approximate the escape widths, $\gamma_n^{\uparrow}$ and $\gamma_p^{\uparrow}$, as

$$\gamma^{\uparrow}(E) = \frac{(2s+1)m}{\pi^2\hbar^2}\pi R^2 \frac{(E-B-V_B)^2}{2gE} \tag{19}$$

where m is the nucleon mass, $s = 1/2$ is the nucleon spin, B_n and B_p are the neutron and proton separation energies, the nuclear radius is taken to be $R = 1.2A^{1/3}$ and the emission barrier is taken to be 0 for neutrons and $V_B = 1.44 * Z/(1.25A^{1/3})$ for protons.

Acknowledgements EVC acknowledges financial support from grants 2016/07398-8 and 2017/13693-5 of the São Paulo Research Foundation (FAPESP). BVC acknowledges financial support from grant 2017/05660-0 of the São Paulo Research Foundation (FAPESP) and grant 306433/2017-6 of CNPq. EVC and BVC acknowledge support from the INCT-FNA project 464898/2014-5. This work is performed in part under the auspices of the U.S. Department of Energy by Lawrence Livermore National Laboratory under Contract DE-AC52-07NA27344 with support from LDRD project 19-ERD-017.

References

1. S. Qaim, F. Tárkányi, R. Capote, *Nuclear Data for the Production of Therapeutic Radionuclides*. No. 473 in Technical Reports Series (International Atomic Energy Agency, Vienna, 2012)
2. G.B. Saha, *Physics and Radiobiology of Nuclear Medicine* (Springer Verlag, New York, 2013)
3. R.H. Cyburt, B.D. Fields, K.A. Olive, T.H. Yeh, Rev. Mod. Phys. **88**, 015004 (2016)
4. M. Dupuis, The European Physical Journal A **53**(5), 111 (2017)
5. G.P.A. Nobre, F.S. Dietrich, J.E. Escher, I.J. Thompson, M. Dupuis, J. Terasaki, J. Engel, Phys. Rev. C **84**, 064609 (2011)
6. J.E. Escher, J.T. Burke, R.O. Hughes, N.D. Scielzo, R.J. Casperson, S. Ota, H.I. Park, A. Saastamoinen, T.J. Ross, Phys. Rev. Lett. **121**, 052501 (2018)
7. A. Ratkiewicz, J.A. Cizewski, J.E. Escher, G. Potel, J.T. Burke, R.J. Casperson, M. McCleskey, R.A.E. Austin, S. Burcher, R.O. Hughes, B. Manning, S.D. Pain, W.A. Peters, S. Rice, T.J. Ross, N.D. Scielzo, C. Shand, K. Smith, Phys. Rev. Lett. **122**, 052502 (2019)
8. H. Fesbach, *Theoretical nuclear physics: Nuclear reactions* (John Wiley and Sons, Inc., 1992)
9. J. Raynal, Computing as a Language of Physics (IAEA, 1972)
10. J. Raynal, Notes on ECIS94, CEA Saclay Report CEA-N-2772 (1994)
11. G. Colò, L. Cao, N. Van Giai, L. Capelli, Computer Physics Communications **184**(1), 142 (2013). DOI 10.1016/j.cpc.2012.07.016
12. E. Chabanat, P. Bonche, P. Haensel, J. Meyer, R. Schaeffer, Nuclear Physics A **635**(1), 231 (1998)
13. E. Chabanat, P. Bonche, P. Haensel, J. Meyer, R. Schaeffer, Nuclear Physics A **643**(4), 441 (1998)
14. E.V. Chimanski, B.V. Carlson, R. Capote, A.J. Koning, Phys. Rev. C **99**, 014305 (2019)

15. A. Koning, J. Delaroche, Nuclear Physics A **713**(3), 231 (2003)
16. A. Nadasen, P. Schwandt, P.P. Singh, W.W. Jacobs, A.D. Bacher, P.T. Debevec, M.D. Kaitchuck, J.T. Meek, Phys. Rev. C **23**, 1023 (1981)
17. A.A. Cowley, A. van Kent, J.J. Lawrie, S.V. Förtsch, D.M. Whittal, J.V. Pilcher, F.D. Smit, W.A. Richter, R. Lindsay, I.J. van Heerden, R. Bonetti, P.E. Hodgson, Phys. Rev. C **43**, 678 (1991)
18. E.V. Chimanski, R. Capote, B.V. Carlson, A.J. Koning, Proceedings CNR*18 (2019)
19. N. Frazier, B.A. Brown, V. Zelevinsky, Phys. Rev. C **54**, 1665 (1996). DOI 10.1103/PhysRevC.54.1665
20. H. Nishioka, H. Weidenmüller, S. Yoshida, Annals of Physics **183**(1), 166 (1988)
21. C.A. Soares Pompeia, B.V. Carlson, Phys. Rev. C **74**, 054609 (2006). DOI 10.1103/PhysRevC.74.054609
22. C. Cline, M. Blann, Nuclear Physics A **172**(2), 225 (1971)
23. A. Koning, M. Duijvestijn, Nuclear Physics A **744**, 15 (2004)
24. J. Dobeš, E. Běták, Nuclear Physics A **272**(2), 353 (1976)